HHS Public Access

Author manuscript

Cell Rep. Author manuscript; available in PMC 2016 August 31.

Published in final edited form as:

Cell Rep. 2016 August 2; 16(5): 1416–1430. doi:10.1016/j.celrep.2016.06.087.

A stem cell model of the motor circuit uncouples motor neuron death from hyperexcitability induced by SMN deficiency

Christian M. Simon[1,2,†], **Anna M. Janas**[1,2,†], **Francesco Lotti**[1,2], **Juan Carlos Tapia**[4,5], **Livio Pellizzoni**[1,2,*], and **George Z. Mentis**[1,2,3,*]

[1]Center for Motor Neuron Biology and Disease, Columbia University, New York, NY, 10032

[2]Department of Pathology and Cell Biology, Columbia University, New York, NY, 10032

[3]Department of Neurology, Columbia University, New York, NY, 10032

[4]Department of Neuroscience, Columbia University, New York, NY, 10032

Summary

In spinal muscular atrophy—a neurodegenerative disease caused by ubiquitous deficiency in the survival motor neuron (SMN) protein—sensory-motor synaptic dysfunction and increased excitability precede motor neuron (MN) loss. Whether central synaptic dysfunction and MN hyperexcitability are cell autonomous events or they contribute to MN death is unknown. We addressed these issues using a stem cell-based model of the motor circuit consisting of MNs and both excitatory and inhibitory interneurons (INs) in which SMN protein levels are selectively depleted. We show that SMN deficiency induces selective MN death through cell autonomous mechanisms, while hyperexcitability is a non-cell autonomous response of MNs to defects in pre-motor INs leading to loss of glutamatergic synapses and reduced excitation. Findings from our *in vitro* model suggest that dysfunction and loss of MNs result from differential effects of SMN deficiency in distinct neurons of the motor circuit and that hyperexcitability does not trigger MN death.

Graphical abstract

[*]Correspondence to: George Z. Mentis (gzmentis@columbia.edu) or Livio Pellizzoni (lp2284@cumc.columbia.edu).
[†]Equal contribution
[5]Current address: Department of Biomedical Sciences, University of Talca, Talca, Chile.

Authors Contribution

GZM and LP conceived and supervised the study. CMS, AMJ, FL and JCT performed experiments. All authors analyzed the data and contributed towards writing the manuscript.

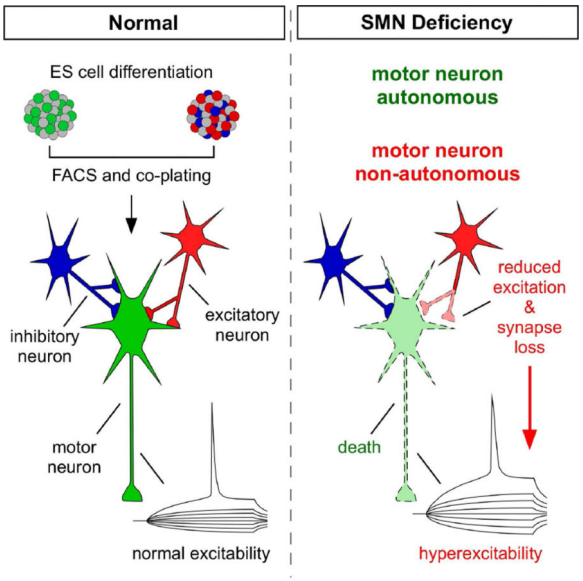

Introduction

Movement is a fundamental behavior produced by contraction of muscles in response to motor neuron (MN) activity. This requires the finely tuned balance of excitatory and inhibitory synaptic drive onto spinal MNs, which is controlled by a variety of synaptic inputs from descending motor pathways, proprioceptive sensory neurons, and local interneurons (INs) of the spinal motor circuit (Arber, 2012). Perturbations in any one element of the motor circuit can have deleterious effects on motor output and are often associated with human disease. Accordingly, degeneration of neurons in brain regions that have modulatory roles in the control of movement underlies motor symptoms in Parkinson's (PD) and Huntington's (HD) disease (Blesa and Przedborski, 2014; Yasuda et al., 2013), while loss of spinal MNs characterizes amyotrophic lateral sclerosis (ALS) (Saxena and Caroni, 2011) and spinal muscular atrophy (SMA) (Tisdale and Pellizzoni, 2015) among other MN disorders. Although the loss of specific neuronal populations is a hallmark of neurodegenerative diseases and the functional properties of vulnerable neurons are often altered prior to death, the basis for the selective vulnerability and the link between dysfunction and death of vulnerable neurons are poorly understood.

In recent years, increasing attention has been given to the possibility that synaptic dysfunction within neural networks is an early, initiating event of disease pathogenesis possibly leading to neuronal death (Caviness, 2014; Li et al., 2003; Marcello et al., 2012; Palop and Mucke, 2010). For instance, alterations of basal ganglia circuitry that lead to deficits in motor control and cognitive processes precede loss of substantia nigra neurons in PD (Meredith and Kang, 2006; Muller et al., 2013) and striatal spiny neurons in HD (Mazarakis et al., 2005; Milnerwood and Raymond, 2007; Usdin et al., 1999), respectively. These and other findings support a network dysfunction model in which disruption of neuronal circuits might be a critical component to disease progression prior to neuronal loss (Palop et al., 2006). In this context, SMA - the most common inherited cause for infant

mortality - has recently emerged as a model to investigate the impact of circuit dysfunction in neurodegenerative disease (Mentis et al., 2011; Imlach et al., 2012; Lotti et al., 2012; Roselli and Caroni, 2012; Tisdale and Pellizzoni, 2015).

SMA is caused by a ubiquitous deficiency in the survival motor neuron (SMN) protein and is characterized by loss of MNs and skeletal muscle atrophy (Tisdale and Pellizzoni, 2015). Through selective depletion and restoration of SMN in specific cell types, several studies revealed that MN death is a cell autonomous process induced by SMN deficiency, which alone cannot account for the SMA phenotype (Gogliotti et al., 2012; Martinez et al., 2012; McGovern et al., 2015). Importantly, dysfunction in other neurons is emerging as an important determinant of motor system pathology in SMA models (Mentis et al., 2011; Imlach et al., 2012; McGovern et al., 2015), while intrinsic muscle deficits do not play a major role (Iyer et al., 2015). In SMA mice, there is a reduction in excitatory but not inhibitory inputs on SMA MNs (Ling et al., 2010; Mentis et al., 2011), and these central synaptic abnormalities are associated with altered sensory-motor neurotransmission and increased intrinsic excitability of MNs, which precedes death of vulnerable MNs (Mentis et al., 2011). Interestingly, increased neuronal excitability is a pathogenic feature common to several neurodegenerative diseases (Bories et al., 2007; Busche et al., 2008; Chan et al., 2007; Palop et al., 2007; Zeron et al., 2002). For instance, compromised afferent connectivity and increased excitability are observed in striatal neurons of HD mouse models (Klapstein et al., 2001), and MN hyperexcitability in mouse models (Bories et al., 2007; Leroy et al., 2014; Quinlan et al., 2011) and cortical hyperexcitability in patients (Vucic et al., 2008) have been linked to neuronal dysfunction in ALS. However, whether hyperexcitability plays a direct causal role in the degeneration of vulnerable neurons is yet to be established, and it remains possible that increased neuronal excitability represents a neuroprotective response to degenerative processes driven by network dysfunction (Palop et al., 2006; Saxena and Caroni, 2011). Understanding the relationship between neural circuit abnormalities, synaptic dysfunction and selective neuronal death may therefore elucidate neurodegenerative disease mechanisms and reveal therapeutic strategies.

Here, we sought to define the cell autonomous and non-cell autonomous requirements of SMN for the survival and function of MNs within the motor circuit. To do so, we established a simplified *in vitro* model of the motor circuit comprising MNs and both excitatory and inhibitory INs differentiated from mouse embryonic stem (ES) cells in which SMN levels can be selectively regulated by RNAi. This system not only recapitulated key pathological changes induced by SMN deficiency *in vivo* such as membrane hyperexcitability and death of SMA MNs, but also enabled us to determine the cellular basis of these phenotypes. Our findings indicate that hyperexcitability and death of SMN-deficient MNs are independent events, resulting from the differential effects of SMN deficiency in distinct neurons of the motor circuit. Furthermore, they implicate altered balance of excitation to inhibition from premotor INs in the SMN-dependent changes of MN excitability. Beyond establishing a stem cell-based platform for the study of SMA disease mechanisms, these results shed light on the origin and causal sequence of events underlying motor circuit dysfunction and MN death induced by SMN deficiency.

Results

Development of ES cells with inducible SMN knockdown

To investigate the effects of SMN deficiency in MNs, we generated a cellular model with drug-inducible, RNAi-mediated knockdown of endogenous Smn in mouse ES cells. First, ES(Hb9::GFP) cells (Wichterle et al., 2002) were transduced with a lentivirus expressing the tetracycline-regulated repressor protein (TetR) and the neomycin resistance gene under the control of the constitutively active PGK promoter (Fig. 1A). A neomycin-resistant clone with high TetR expression was isolated and then transduced with a lentivirus that expresses a short hairpin RNA (shRNA) against mouse Smn mRNA under the control of a modified H1 promoter containing the Tet operator (TO) sequences as well as the puromycin resistance gene driven by the PGK promoter (Fig. 1A), which was followed by puromycin selection to isolate clonal ES(Hb9::GFP)-Smn_{RNAi} cells. The constitutively expressed TetR protein binds to the TO sequences and represses shRNA expression. Addition of the tetracycline analog doxycycline (Dox) to the growth media relieves TetR protein binding and induces Smn shRNA expression (Lotti et al., 2012).

RNA and protein analysis from control (WT) and Smn_{RNAi} (RNAi) ES cells cultured in the presence or absence of Dox for 4 days showed a strong decrease in Smn mRNA and protein levels in Dox-treated relative to untreated RNAi cells, while Dox treatment had no effect on Smn levels in WT cells (Fig. 1B–C). Importantly, following ES-Smn_{RNAi} differentiation into MNs, Dox treatment for 5 days induced a decrease in Smn mRNA and protein to approximately 10% of normal levels (Fig. 1D–E), which is comparable to SMN expression in tissues of severe SMA mice (Gabanella et al., 2007).

To control for potential shRNA off-target effects, we generated an additional cell line ES(Hb9::GFP)-SMN/Smn_{RNAi} by transducing ES-Smn_{RNAi} cells with a lentivector expressing epitope-tagged human SMN (hSMN) under the control of the ubiquitous PGK promoter and the hygromycin resistance gene driven by the SV40 promoter (Fig. S1A). RT-qPCR and Western blot analysis of both ES and ES-derived MNs from this cell line revealed both hSMN expression and a reduction of endogenous Smn similar to that in the parental Smn_{RNAi} cell line following Dox treatment (Fig. S1B–E). Furthermore, since the shRNA specifically targets mouse but not human SMN (Lotti et al., 2012), hSMN was unaffected by Dox treatment and was found to accumulate to ~15–20% the levels of endogenous Smn (Fig. S1C and S1E). Importantly, ES(Hb9::GFP) cells express GFP driven by the Hb9 promoter following directed differentiation into MNs (Wichterle et al., 2002) and both Smn_{RNAi} and SMN/Smn_{RNAi} ES cells retained the ability to differentiate into MNs with an efficiency similar to the parental wild type cell line as determined by FACS analysis (Fig. S1F).

In summary, we established ES cell lines with drug-inducible knockdown of endogenous Smn. The regulated expression of Smn combined with the MN-specific expression of GFP provides a powerful platform to study the effects of SMN deficiency on MN survival and function.

Smn deficiency leads to cell-autonomous death of MNs

Since MN loss is a hallmark in SMA (Tisdale and Pellizzoni, 2015), we investigated whether Smn deficiency induces death of MNs in our model system by comparing the survival of MNs differentiated from WT and RNAi ES cells. To do so, ES-MNs dissociated from embryoid bodies (EBs), which contain ~25% MNs together with both neuronal and non-neuronal cells (Fig. S1F), were plated into 96-well plates and cultured in the presence or absence of Dox for up to 5 days. MN number was determined daily using automated, high-throughput image collection of complete wells (Fig. 1F) followed by analysis with the MetaMorph software to selectively identify and count the number of GFP+ cells (Fig. 1G). While Dox treatment had no effect on the survival of MNs differentiated from WT ES cells, Dox-treated Smn-deficient MNs differentiated from RNAi ES cells exhibited a significant time-dependent decrease in survival relative to untreated MNs with normal Smn levels (Fig. 1H). Importantly, Dox-treated MNs differentiated from ES-SMN/Smn_{RNAi} cells had a survival comparable to that of WT MNs (Fig. 1H), indicating that the relatively low levels of hSMN expression in ES-SMN/Smn_{RNAi} cells were sufficient to correct the survival deficits induced by Smn deficiency in ES-MNs, and that these deficits are SMN-dependent. While seemingly surprising, the restoration of ES-MN survival by a two-fold increase in SMN levels is consistent with *in vivo* studies showing that SMN-dependent phenotypes are strongly dependent on the reduction of SMN protein below a critical threshold and that a small increase in SMN dosage can have a dramatic biological impact as indicated by the analysis of *Smn* knockout mice harboring an allelic series of hypomorphic *SMN2* genes (Osborne et al., 2012).

Next, we analyzed IN survival by counting the number of $Tuj1^{+}/GFP^{-}$ neurons differentiated from RNAi ES cells (Fig. S1G) and found no significant loss of SMN-deficient INs relative to controls after 5 days in culture (Fig. S1H), highlighting the selectivity of the effects of SMN deficiency on MN survival. Lastly, we investigated whether the effect of SMN deficiency on ES-MN survival was mediated by cell autonomous or non-cell autonomous mechanisms. To do so, we carried out survival analysis of GFP^{+} MNs differentiated from either WT or RNAi ES cells following their FACS purification to greater than 95% purity (Fig. S1I–J). Smn deficiency induced death of purified MNs to a rate and extent similar to that of MNs in mixed cultures with other neurons and non-neuronal cells (Fig. 1I), while FACS-purified Dox-treated MNs differentiated from ES-SMN/Smn_{RNAi} cells had a survival comparable to that of WT MNs (Fig. 1I), indicating that hSMN expression in purified SMN-deficient MNs rescued neuronal death.

Together, these results demonstrate that our stem cell model recapitulates the selective death of MNs induced by Smn deficiency, which is a key feature of the disease in both humans and mouse models. They further indicate that cell-autonomous mechanisms are responsible for the death of Smn-deficient MNs *in vitro*.

Smn deficiency induces MN hyperexcitability by non-cell autonomous mechanisms

Increased membrane excitability is an early physiological signature of dysfunction that precedes MN death in mouse models of SMA (Mentis et al., 2011). However, the cellular basis of this physiological perturbation and its relationship with MN death are unknown. To

address these issues, we used whole cell patch clamp recordings to study the functional characteristics of ES-derived MNs with either normal or reduced levels of Smn. MNs differentiated from WT and RNAi ES cells were cultured in the presence or absence of Dox for 5 days and then visually-targeted based on GFP expression for intracellular recordings, after which they were filled with a fluorescent dye for *post hoc* morphological analysis (Fig. 2A). Remarkably, while the resting membrane potential of MNs did not reveal any significant differences between groups (Table S1), two passive membrane properties of input resistance and time constant were significantly increased in Dox-treated Smn-deficient MNs relative to untreated MNs differentiated from RNAi ES cells (Fig. 2B–C). Dox-treatment had no effect on the intrinsic membrane properties of MNs differentiated from WT ES cells that have normal Smn levels (Fig. S2A–C) and hSMN expression corrected the changes in both input resistance and time constant in Smn-deficient MNs differentiated from ES-SMN/Smn_{RNAi} cells (Fig. S2D–F), demonstrating that these physiological alterations are SMN-dependent.

To determine if increased excitability reflects intrinsic, cell autonomous changes induced by SMN deficiency in MNs, we performed electrophysiological recordings in FACS-purified MNs differentiated from RNAi ES cells (Fig. S1I–J). We found that purified, Smn-deficient MNs did not exhibit any significant differences in either input resistance or time constant, nor any changes in resting membrane potential compared to controls with normal Smn levels (Fig. 2D–F, Table S1), indicating that hyperexcitability is independent of Smn reduction in MNs.

Together, these results demonstrate that Smn deficiency alters the intrinsic membrane properties of ES-derived MNs *in vitro*, inducing a state of hyperexcitability akin to the functional changes observed in SMA MNs *in vivo* (Mentis et al., 2011). Moreover, they indicate that Smn deficiency induces MN hyperexcitability through non-cell autonomous mechanisms that are likely distinct from the cell autonomous mechanisms that result in MN death.

SMN deficiency does not alter the somato-dendritic area of MNs

Next, we sought to investigate the mechanisms responsible for the MN excitability changes induced by SMN deficiency. Soma size, dendritic tree area and specific membrane resistivity are among the key parameters governing the intrinsic membrane properties of MNs (Kernell, 1966; Mentis et al., 2007). Therefore, we first investigated if changes in hyperexcitability could be due to a Smn-dependent reduction in the somato-dendritic area of MNs. To do so, we acquired confocal images of intracellularly filled MNs following electrophysiological recordings, which we reconstructed and analyzed using Neurolucida software (Fig. 3A and 3C). Tracing analysis revealed no changes in total dendritic area, length or number of primary dendrites and number of dendritic ends between Smn-deficient and control MNs in mixed (Fig. 3B and Fig. S3A) or FACS-purified (Fig. 3D and Fig. S3B) cultures. Additionally, there was no difference in transverse soma area between the two groups (Fig. 3B and 3D). The lack of morphological changes in dendritic tree and soma area was also consistent with the observation that the capacitance - a physiological readout of membrane area - was not significantly different between control and Smn-deficient MNs (Fig. 3B and

3D, Table S1). Notably, however, FACS MNs possess a dendritic tree of much lower complexity compared to MNs in mixed cultures (Fig. 3). This strong reduction in dendritic complexity is neither dependent on SMN expression nor due to the FACS procedure, but rather the effect of MNs being cultured in isolation (see also Fig. S5C–D). Together these results demonstrate that morphological changes in the somato-dendritic area of MNs do not contribute to their increased excitability upon SMN depletion.

Development of ES cell lines for the purification of INs with inducible SMN knockdown

To investigate the possibility that MN hyperexcitability represents a response to dysfunction of Smn-deficient premotor INs, we developed a purified co-culture system in which the effects of selective reduction of Smn in either MNs or INs could be specifically dissected.

First, we modified our mouse ES cell lines to fluorescently label and sort INs following neuronal differentiation. TetR-expressing WT and RNAi ES(Hb9::GFP) cells were transduced with a lentiviral construct expressing mCherry under the control of the pan-neuronal mouse Synapsin 1 (Syn1) promoter, which has been shown to drive efficient and specific expression of transgenes in neurons (Kugler et al., 2001), and the hygromycin resistance gene expressed from the SV40 promoter for antibiotic selection (Fig. 4A). To validate the specificity of mCherry expression in neurons, retinoic acid (RA) was used to differentiate WT and RNAi ES(Hb9::GFP; Syn::mCherry) cell lines to neurons, which we then immunostained with the pan-neuronal Tuj1 antibody (Fig. 4B). We found that more than 95% of $Tuj1^+$ neurons co-expressed mCherry, which had marginal, if any, expression in non-neuronal cells (Fig. 4C).

Next, we cultured WT and RNAi ES(Hb9::GFP; Syn::mCherry) cells for 5 days in the presence or absence of Dox and found that Dox treatment induced a strong reduction in both Smn mRNA and protein levels in RNAi but not WT cells (Fig. 4D–E). Further, a similar Dox-dependent Smn knockdown was also seen after neuronal differentiation of RNAi but not WT ES(Hb9::GFP; Syn::mCherry) cells (Fig. 4F–G). Thus, both the specificity and extent of Smn knockdown was analogous to that observed in their respective parental cell lines (compare Figs. 1B–E and 4D–G).

Directed differentiation of ES cells in the presence of RA can yield spinal INs, the exact identity of which has not been established. Since spinal motor circuits *in vivo* comprise both excitatory and inhibitory inputs that converge onto MNs to modulate their function (Arber, 2012), we investigated the neurotransmitter identity of INs differentiated from mouse ES cells. Importantly, mCherry+ INs can be differentiated from ES(Hb9::GFP; Syn::mCherry) cells with high efficiency in the presence of RA and isolated by FACS to greater than 95% purity and with essentially no MN contamination (Fig. S4A–D). We performed RT-qPCR experiments on RNA extracted from ES-derived, FACS-purified INs and MNs to measure the relative enrichment of all three glutamatergic vesicular transporters (VGluT1, 2, 3), the vesicular GABA transporter (VGAT), the neuronal glycine transporter (GlyT2) and the cholinergic transporter (VAChT). We also monitored expression of the pan-neuronal markers Syn1 and Synaptophysin (Syp) as well as the MN-specific markers Hb9 and choline acetyl transferase (ChAT). We found that purified INs and MNs express similar levels of Syn1 and Syp (Fig. S4E), while the cholinergic markers VAChT and ChAT as well as the MN-specific

transcription factor Hb9 are highly expressed in MNs but not in INs (Fig. S4F). Conversely, INs express significantly higher levels of VGluT2, VGAT, and GlyT2 mRNAs relative to MNs (Fig. S4G). RT-qPCR also indicated that VGluT1 and VGluT3 mRNAs as well as dopaminergic and serotonergic markers are not expressed in INs (Fig. S4G and data not shown).

In summary, we established an ES cell-based system to fluorescently identify and efficiently purify excitatory (VGluT2) and inhibitory (VGAT and GlyT2) INs with regulated knockdown of SMN.

Smn deficiency in pre-motor INs induces MN hyperexcitability

To determine the cellular basis of MN dysfunction induced by SMN deficiency, we developed a simplified *in vitro* model of the motor circuit that took advantage of our ability to isolate ES cell-derived MNs and INs and to knockdown Smn selectively in either neuronal type. We co-cultured FACS-purified GFP^+ MNs derived from WT or RNAi ES(Hb9::GFP) cells with FACS-purified $mCherry^+/GFP^-$ INs derived from WT or RNAi ES(Hb9::GFP; Syn::mCherry) cells (Fig. 5A). MNs and INs were co-plated at a 1 to 5 ratio (the same found in mixed cultures) and cultured for 5 days in the presence of Dox prior to electrophysiological analysis (Fig. 5A–B). Western blot analysis confirmed robust, Dox-dependent Smn knockdown in FACS-purified MNs and INs differentiated from RNAi but not WT ES cell lines under these experimental conditions (Fig. S5A).

We investigated the Smn-dependent functional changes in MNs co-cultured with INs in the following four different combinations (Fig. 5A): i) WT MNs with WT INs; ii) Smn-deficient MNs with Smn-deficient INs; iii) Smn-deficient MNs with WT INs; and iv) WT MNs with Smn-deficient INs. Following patch clamp studies to determine their physiological parameters, MNs were subsequently filled for morphological studies (Fig. 5B) and tracing analysis using Neurolucida revealed that the extent and complexity of the dendritic arborization of FACS-purified MNs co-cultured with INs is similar to that of MNs in mixed cultures (Fig. S5C–D). While MN resting potential was unchanged in all combinations (Table S1), analysis of co-cultures of Smn-deficient MNs and INs compared to WT co-cultures revealed an increase in input resistance and time constant of MNs (Fig. 5C–D) similar to that found in mixed cultures (see also Fig. 2B–C). Next, we investigated the intrinsic properties of Smn-deficient MNs co-plated with WT INs and found no significant difference in either input resistance or time constant (Fig. 5C–D). In marked contrast, the intrinsic properties of WT MNs co-plated with Smn-deficient INs were significantly altered as indicated by the increases in both input resistance and time constant (Fig. 5C–D). These results demonstrate that Smn deficiency in INs induces non-cell autonomous dysfunction of MNs by increasing their intrinsic membrane excitability.

Smn deficiency in INs leads to loss of excitatory synapses onto MNs

The intrinsic mechanisms by which SMN-deficient INs elicit hyperexcitability of MNs is unknown. Consistent with the loss of excitatory glutamatergic synapses onto MNs observed in SMA mice (Ling et al., 2010; Mentis et al., 2011), one possibility is that decreased excitatory presynaptic input from INs may contribute to MN dysfunction in our model of the

motor circuit. To address this, we investigated the effects of Smn depletion on synaptic inputs from pre-motor INs onto MN somata and dendrites by immunostaining of synapses that impinge on intracellularly-filled MNs described in Figure 5. Synapses were identified by immunoreactivity against the pan-synaptic marker Syp and either VGluT2 to label excitatory synapses (Fig. 6A–B) or VGAT to label inhibitory GABAergic synapses (Fig. 6D–E), while we were unable to detect GlyT2 synapses with available antibodies.

To further validate the identity of Syp^+ puncta as *bona fide* synaptic connections, we used antibodies against PSD95 and Gephyrin to investigate post-synaptic specialization of excitatory and inhibitory synapses, respectively. As expected, we found that Syp^+ boutons are opposed to both PSD95 and Gephyrin on somata and dendrites of MNs (Fig. S6A–B). Greater than 90% of Syp^+ boutons onto MNs had a post-synaptic specialization with ~70% being opposed to PSD95 and ~20% to Gephyrin (Fig. S6C). In addition, $VGluT2^+$ boutons are opposed to PSD95, but not to Gephyrin (data not shown), demonstrating proper specificity in the specialization of excitatory synapses. Lastly, we investigated the ultra-structural features of the synapses established in co-cultures of MNs and INs by electron microscopy (EM) analysis of intracellularly filled MNs at 5DIV (Fig. S6D–G). The EM showed that somata and dendrites of MNs receive presynaptic boutons containing neurotransmitter vesicles, mitochondria, and active zones (Fig. S6G), further corroborating the formation of proper synaptic connections in our *in vitro* model of the motor circuit.

In cultures with normal levels of SMN, $VGluT2^+$ excitatory synapses constituted ~40% and ~30% of the total number of synapses, respectively, on MN soma and dendrites (Fig. 6C). Importantly, SMN deficiency in both INs and MNs caused a ~80% reduction of VGluT2 synapses on soma and ~70% reduction on dendrites of MNs (Fig. 6A–C). In contrast, the number of GABAergic synapses, which constitute ~15% of the total number of synapses onto MNs, was not significantly altered by Smn depletion (Fig. 6D–F), demonstrating the specificity of the effects for excitatory synapses. Furthermore, RT-qPCR experiments revealed that SMN deficiency does not alter the expression of VGluT2 as well as VGAT, GlyT2, and Syn1 mRNAs in purified INs (Fig. S5B). Thus, the SMN-dependent reduction in VGluT2 synapses cannot be attributed to either down-regulation of VGluT2 mRNA expression or death of INs.

Next, we investigated whether the selective loss of glutamatergic synapses was dependent on Smn-deficiency in MNs, INs or both. We quantified the synaptic coverage of VGluT2 synapses in co-cultures of Smn-deficient MNs with WT INs and *vice versa*. Remarkably, we found that the number of VGluT2 synapses on both somata and dendrites of MNs was decreased when Smn-deficient INs were co-cultured with normal MNs, while it was not affected when normal INs were co-cultured with Smn-deficient MNs (Fig. 6C). Therefore, the reduction in VGluT2 synapses was specifically due to the effects of Smn deficiency in INs but not MNs. Collectively, these results identify the loss of VGluT2 synapses on MNs as an intrinsic defect induced by SMN deficiency in excitatory INs, which in turn may trigger homeostatic changes of MN excitability through a reduction in the excitatory drive.

Block of excitatory neurotransmission induces hyperexcitability but not death of MNs

Our findings implicate dysregulation of synaptic activity of excitatory pre-motor INs as a non-cell autonomous mechanisms contributing to the increased excitability of MNs induced by SMN deficiency. Therefore, we used pharmacological assays to investigate whether altered excitatory synaptic drive can modify the intrinsic membrane excitability of MNs *in vitro*. First, we chronically applied Tetrodotoxin (TTX) in mixed cultures of ES-derived WT MNs to inhibit the firing of action potentials in neurons and to study the effect of global silencing of neuronal activity. Patch-clamp recordings revealed that in response to TTX, WT MNs exhibited a ~25% increase in both input resistance and time constant at 5DIV (Fig. 7A–B), while resting potential, soma area and capacitance were unchanged (Table S1). TTX treatment did not cause a further increase in the input resistance of Smn-deficient MNs (Fig. S7). Together these findings reveal that TTX-dependent silencing of synaptic transmission leads to an activity-dependent increase in excitability of WT MNs.

Next, we determined the relative contribution of excitatory, inhibitory and cholinergic synaptic drive to MN excitability through selective neurotransmission blockade. Mixed cultures of ES-MNs were treated daily with either glutamatergic (NBQX and APV), cholinergic (atropine, mecamylamine and dHBE), glycinergic (strychnine) or GABAergic (bicuculline) receptor blockers and recordings were performed at 5DIV in the presence of these blockers. Strikingly, while blocking cholinergic or inhibitory neurotransmission had no effect on the intrinsic properties of MNs (Fig. 7A–B), glutamatergic receptors blockade increased both input resistance and time constant of WT ES-MNs to an extent comparable to that of chronic TTX treatment (Fig. 7A–B and Table S1). No changes in resting potential, soma area or capacitance were found in any of these conditions (Table S1).

Lastly, we investigated the effect of treatment with neurotransmitter blockers on MN survival. Time-course analysis of MN survival in the presence of vehicle or pharmacological blockers at the same concentrations used for electrophysiology studies showed that neither TTX nor any of the neurotransmitter receptor blockers enhanced MN loss relative to vehicle-treated controls (Fig. 7C).

Collectively, these results reveal that excitatory glutamatergic neurotransmission plays a key role in governing the intrinsic properties of MNs and that its reduction phenocopies the increased excitability induced by Smn deficiency in cultured MNs. Moreover, hyperexcitability has no significant effects on survival of WT MNs, supporting the conclusion that hyperexcitability and death of Smn-deficient MNs are uncoupled events that are mediated by different mechanisms.

Discussion

The discovery that stem cells can be faithfully differentiated into MNs has provided the foundation for modeling MN diseases such as SMA and ALS *in vitro* as a means to study disease mechanisms and to identify candidate therapeutics. Here, leveraging the power of stem cell-based approaches, we developed an *in vitro* model composed of MNs and both excitatory and inhibitory INs in which the expression of SMN could be selectively regulated to study the requirement for SMN in the motor circuit. Our system recapitulates key

pathological events of SMA, including degeneration and hyperexcitability of MNs. Importantly, we show that death of SMN-deficient MNs is cell autonomous, while MN hyperexcitability occurs through non-cell autonomous mechanisms involving a homeostatic response to synaptic dysfunction of SMN-deficient excitatory INs. Together, our findings provide insights into the cellular basis of MN dysfunction induced by SMN deficiency. They reveal that disrupted excitatory drive alters the intrinsic physiological properties of MNs but that membrane hyperexcitability does not trigger MN death. Thus, dysfunction and death of MNs represent distinct pathogenic events in the SMA motor circuit.

A hallmark of SMA is the loss of MNs, which is observed in both patients and mouse models of the disease (Tisdale and Pellizzoni, 2015). Our findings reveal that SMN deficiency induces selective MN death *in vitro* that is mediated by cell autonomous mechanisms. This is in agreement with previous *in vitro* and *in vivo* studies that used stem cell-derived mouse and human MNs (Ebert et al., 2009; Makhortova et al., 2011; Sareen et al., 2012; Ng et al., 2015) as well as selective restoration of SMN in MNs of SMA mice (Gogliotti et al., 2012; Martinez et al., 2012; McGovern et al., 2015) and conditional SMN depletion from MNs of wild type mice (Park et al., 2010; McGovern et al., 2015). Thus, our model system recapitulates a key feature of the human disease and supports the conclusion that SMN reduction has differential effects on the survival of MNs relative to other types of neurons. While the precise molecular mechanisms remain to be fully elucidated, recent work has implicated selective activation of ER stress in the death pathway of SMA MNs (Ng et al., 2015).

SMN deficiency induces hyperexcitability of MNs in a mouse model of SMA (Mentis et al., 2011) and this early feature of the disease process is also observed in our stem cell model of the motor circuit as well as in human SMA MNs differentiated from induced pluripotent stem cells (Liu et al., 2015). Importantly, our system allowed us to address whether MN hyperexcitability is due to cell autonomous or non-cell autonomous mechanisms induced by SMN deficiency, which was not previously established. We found that SMN deficiency does not induce hyperexcitability in MNs cultured in isolation but requires the presence of INs. Moreover, SMN deficiency in premotor INs is necessary and sufficient to increase excitability of MNs irrespective of their SMN levels. Collectively, these results reveal that MN hyperexcitability is due to non-cell autonomous mechanisms.

Loss of glutamatergic proprioceptive synapses but not inhibitory ones is an early event that coincides with changes in the intrinsic excitability of MNs in SMA mice (Ling et al., 2010; Mentis et al., 2011), but a causal relationship between reduced excitatory drive and hyperexcitability of SMA MNs was not established. Importantly, the presence of both excitatory (VGluT2) and inhibitory (VGAT and GlyT2) INs allowed us to probe this question and the underlying mechanisms responsible for the non-autonomous effects of SMN deficiency on MN hyperexcitability. Similar to observations made in SMA mice (Ling et al., 2010), we found that VGluT2+ synapses from excitatory premotor INs onto MNs are selectively lost under SMN deficiency, while inhibitory synapses are not affected. Further, we show that loss of excitatory synapses is a direct consequence of the effects of SMN deficiency in excitatory INs. Consistent with a reduction of excitatory drive being causally related to MN dysfunction under SMN deficiency, chronic pharmacological blockade of

glutamate receptors–but not inhibitory or cholinergic receptors–significantly increased MN excitability, and a similar result was obtained in experiments in which synaptic activity was abolished by exposure to TTX. Collectively, these results indicate that SMN deficiency results in MN dysfunction via non-cell autonomous mechanisms and identified excitatory INs as key determinants of MN excitability.

Dysfunction of INs has been implicated in Alzheimer's disease (Palop and Mucke, 2010), schizophrenia (O'Donnell, 2012; Sigurdsson, 2015) and autism (Port et al., 2014; Uhlhaas and Singer, 2012; Zoghbi and Bear, 2012). Our findings implicate disruption of excitatory drive from premotor INs in the functional alterations induced by SMN deficiency in the mammalian motor circuit and identify hyperexcitability of SMN-deficient MNs as a homeostatic response to defective glutamatergic neurotransmission. Since experience refines the properties of neural circuits via activity-dependent alterations in the number, strength and type of synapses (Ganguly and Poo, 2013; Yin and Yuan, 2014), an imbalance of inhibitory and excitatory synaptic activity on MNs would likely impact their intrinsic membrane properties. The intrinsic membrane properties of MNs determine how converging premotor synaptic drive is translated into the final motor command transmitted to muscles (Powers and Binder, 2001). To this end, blocking synaptic activity with TTX in cultured rat pyramidal neurons leads to increased intrinsic excitability (Desai et al., 1999). In addition, genetic ablation of glutamatergic synaptic transmission onto individual CA1 pyramidal neurons *in vivo* causes homeostatic adaptation by strongly increasing neuronal excitability without perturbing neuronal morphology (Lu et al., 2013). Accordingly, we find that SMN deficiency induces hyperexcitability but does not alter either soma size or the extent of the dendritic tree of MNs. Altogether, these results point to an indirect role for SMN in shaping the membrane excitability of MNs through the control of neural network activity and excitatory synaptic neurotransmission in the motor circuit. Further, they support the possibility that excitatory/inhibitory imbalance induced by SMN deficiency is an initiating event leading to the functional disruption of the SMA motor circuit.

MN hyperexcitability has often been linked to neuronal death. In a model of cerebral ischemia, selective death of hippocampal pyramidal neurons correlated with increased input resistance of ischemic neurons (Fan et al., 2008). Similarly, axotomy of facial or spinal MN axons in neonatal rats causes significant loss of MNs early after the disconnection with their muscle targets (Mentis et al., 2007; Umemiya et al., 1993), with the marked increase in input resistance of a subpopulation of axotomized MNs being interpreted as a "pre-lethal" stage (Umemiya et al., 1993). Further, changes in MN excitability have also been associated with neuronal death in ALS (Devlin et al., 2015; Wainger et al., 2014). Stem cell-derived ALS MNs exhibit increased firing frequencies mediated by changes in the activity of Kv7 potassium channels and reduced survival, both of which are reversed by treatment with the Kv7 antagonist retigabine (Wainger et al., 2014). To date, however, a cause-effect relationship between hyperexcitability and death of MNs has not been conclusively established. Here, we provide direct evidence that hyperexcitability and death of MNs are two independent, causally unrelated events induced by SMN deficiency in the motor circuit. First, MNs degenerate due to intrinsic, cell-autonomous mechanisms triggered by SMN deficiency, while MN hyperexcitability results from dysfunction of excitatory premotor INs. Second, SMN deficiency induces death of purified MNs in culture without changing their

intrinsic excitability. Lastly, either silencing all synaptic activity with TTX or selectively blocking glutamatergic transmission increases excitability of wild type MNs without inducing their death. Thus, our work reveals that hyperexcitability is not in itself a trigger of MN death. On the contrary, we believe it reflects a homeostatic attempt of MNs to counteract the decrease in the excitatory drive received from premotor INs. According to this scenario, and consistent with findings in a *Drosophila* SMA model (Imlach et al., 2012; Lotti et al., 2012), correction of the functional properties of MNs in mouse models of SMA will likely require SMN restoration in glutamatergic neurons of the motor circuit. Direct support to this possibility–further corroborating the predictive power of findings in our *in vitro* model with regard to the *in vivo* situation–comes from studies in a mouse model of SMA in which we find that selective restoration of SMN in glutamatergic neurons that provide direct excitatory drive onto MNs is sufficient to non-autonomously reinstate the normal physiological properties of SMA MNs but not to rescue their survival (Emily Fletcher and G.Z.M., unpublished results). By extension, complete correction of motor function in SMA mice would require SMN restoration in excitatory neurons of the motor circuit in addition to MNs.

In conclusion, our findings point to premotor excitatory synapses as key determinants of MN dysfunction induced by SMN deficiency in the motor circuit and candidate therapeutic targets for SMA. Further, our stem cell-based model of the motor circuit provides a powerful platform to dissect the cascade of SMN-dependent events leading to death and dysfunction of MNs at the synaptic and molecular levels.

Experimental Procedures

ES cell lines and neuronal differentiation

ES cell lines were generated through lentiviral transduction (Lotti et al., 2012). Directed differentiation of ES cells into MNs and INs was carried out according to previously reported protocols (Wichterle et al., 2002). Further details are provided in Supplemental Experimental Procedures.

RNA and protein analysis

Total RNA purification and RT-qPCR analysis were carried out as previously described (Lotti et al., 2012). The primers used are listed in Table S2. Total protein extracts were prepared by homogenization of cells in SDS sample buffer and analyzed by Western blot using the antibodies listed in Table S3.

MN survival

For each independent experiment, whole-well automated image acquisition (600ms exposure) of GFP^+ MNs plated in six replicate wells of 96-well plates per condition was performed using the Flash Cytometer (Trophos) every day from ~12h post plating (0DIV) until day 5 (5DIV) using excitation at 455–490nm and emission at 495–540nm. Cell number in each well was measured using the MetaMorph Neurite Outgrowth Application Module (Molecular Devices) and the average of the six replicate wells determined.

Electrophysiology

MNs were visually targeted by their endogenous GFP fluorescence. We applied standard whole cell patch current clamp protocols and recordings were accepted for analysis only if they met the following criteria: i) stable resting membrane potential of −35mV or lower, and ii) overshooting action potentials. The passive membrane properties of MNs were assessed by injection of negative and positive steps of current pulses (100ms duration) at −60mV holding membrane potential. The input resistance was calculated from the slope of the linear current/voltage relationship.

For pharmacological experiments, TTX (1μM) was added to neuronal cultures and supplemented fresh every day for five days. Specific neurotransmitter receptor blockade was accomplished by using glutamatergic (100μM APV and 20μM NBQX), GABAergic (20μM Bicuculine), glycinergic (1μM Strychnine) and cholinergic (50μM Dihydro-β-erythroidine hydrobromide, 50μM mecamylamine, and 5μM atropine) receptor blockers. Medium was changed every day for five days. Pharmacological blockers were maintained at the same concentration during electrophysiological experiments.

Neuronal reconstructions

Quantification of dendritic tree length, surface area, and complexity was done by manual tracing from single plane confocal images of intracellularly filled MNs using Neurolucida (v10.0, MBF Bioscience). Immunofluorescence analysis and confocal imaging was carried out as described in Supplemental Experimental Procedures.

Statistical analysis

Statistical analysis was carried out using the two-tailed unpaired Student’s t test, one- or two-way ANOVA as applicable, using Prism 5 software (GraphPad). Data are represented as mean and standard error of the mean (SEM) from independent experiments and P values are indicated as follows: * = $P < 0.05$; ** = $P < 0.01$; *** = $P < 0.001$.

Supplementary Material

Refer to Web version on PubMed Central for supplementary material.

Acknowledgments

We would like to thank Drs. Clifford Woolf, Neil Shneider and Hynek Wichterle for critical comments on the manuscript. This work was supported by grants from SMA Europe (GZM and LP); the SMA Foundation (LP); U.S. Department of Defense GR.10235006 (GZM); Fondecyt 1160888 (JCT); and NIH-NINDS R01NS078375 (GZM) and R01NS069601 (LP). CMS was the recipient of Young Investigator award by ROCHE. AMJ was the recipient of a training grant by Columbia University.

References

Arber S. Motor circuits in action: specification, connectivity, and function. Neuron. 2012; 74:975–989. [PubMed: 22726829]

Blesa J, Przedborski S. Parkinson's disease: animal models and dopaminergic cell vulnerability. Front Neuroanat. 2014; 8:155. [PubMed: 25565980]

Bories C, Amendola J, Lamotte d'Incamps B, Durand J. Early electrophysiological abnormalities in lumbar motoneurons in a transgenic mouse model of amyotrophic lateral sclerosis. Eur J Neurosci. 2007; 25:451–459. [PubMed: 17284186]

Busche MA, Eichhoff G, Adelsberger H, Abramowski D, Wiederhold KH, Haass C, Staufenbiel M, Konnerth A, Garaschuk O. Clusters of hyperactive neurons near amyloid plaques in a mouse model of Alzheimer's disease. Science. 2008; 321:1686–1689. [PubMed: 18802001]

Caviness JN. Pathophysiology of Parkinson's disease behavior--a view from the network. Parkinsonism Relat Disord. 2014; 20(Suppl 1):S39–S43. [PubMed: 24262185]

Chan CS, Guzman JN, Ilijic E, Mercer JN, Rick C, Tkatch T, Meredith GE, Surmeier DJ. 'Rejuvenation' protects neurons in mouse models of Parkinson's disease. Nature. 2007; 447:1081–1086. [PubMed: 17558391]

Desai NS, Rutherford LC, Turrigiano GG. Plasticity in the intrinsic excitability of cortical pyramidal neurons. Nat Neurosci. 1999; 2:515–520. [PubMed: 10448215]

Devlin AC, Burr K, Borooah S, Foster JD, Cleary EM, Geti I, Vallier L, Shaw CE, Chandran S, Miles GB. Human iPSC-derived motoneurons harbouring TARDBP or C9ORF72 ALS mutations are dysfunctional despite maintaining viability. Nat Commun. 2015; 6:5999. [PubMed: 25580746]

Ebert AD, Yu J, Rose FF Jr, Mattis VB, Lorson CL, Thomson JA, Svendsen CN. Induced pluripotent stem cells from a spinal muscular atrophy patient. Nature. 2009; 457:277–280. [PubMed: 19098894]

Fan Y, Deng P, Wang YC, Lu HC, Xu ZC, Schulz PE. Transient cerebral ischemia increases CA1 pyramidal neuron excitability. Exp Neurol. 2008; 212:415–421. [PubMed: 18559277]

Gabanella F, Butchbach ME, Saieva L, Carissimi C, Burghes AH, Pellizzoni L. Ribonucleoprotein assembly defects correlate with spinal muscular atrophy severity and preferentially affect a subset of spliceosomal snRNPs. PLoS One. 2007; 2:e921. [PubMed: 17895963]

Ganguly K, Poo MM. Activity-dependent neural plasticity from bench to bedside. Neuron. 2013; 80:729–741. [PubMed: 24183023]

Gogliotti RG, Quinlan KA, Barlow CB, Heier CR, Heckman CJ, Didonato CJ. Motor neuron rescue in spinal muscular atrophy mice demonstrates that sensory-motor defects are a consequence, not a cause, of motor neuron dysfunction. J Neurosci. 2012; 32:3818–3829. [PubMed: 22423102]

Imlach WL, Beck ES, Choi BJ, Lotti F, Pellizzoni L, McCabe BD. SMN is required for sensory-motor circuit function in Drosophila. Cell. 2012; 151:427–439. [PubMed: 23063130]

Iyer CC, McGovern VL, Murray JD, Gombash SE, Zaworski PG, Foust KD, Janssen PM, Burghes AH. Low levels of Survival Motor Neuron protein are sufficient for normal muscle function in the SMNDelta7 mouse model of SMA. Hum Mol Genet. 2015; 24:6160–6173. [PubMed: 26276812]

Kernell D. Input resistance, electrical excitability, and size of ventral horn cells in cat spinal cord. Science. 1966; 152:1637–1640. [PubMed: 5936887]

Klapstein GJ, Fisher RS, Zanjani H, Cepeda C, Jokel ES, Chesselet MF, Levine MS. Electrophysiological and morphological changes in striatal spiny neurons in R6/2 Huntington's disease transgenic mice. J Neurophysiol. 2001; 86:2667–2677. [PubMed: 11731527]

Kugler S, Meyn L, Holzmuller H, Gerhardt E, Isenmann S, Schulz JB, Bahr M. Neuron-specific expression of therapeutic proteins: evaluation of different cellular promoters in recombinant adenoviral vectors. Mol Cell Neurosci. 2001; 17:78–96. [PubMed: 11161471]

Leroy F, Lamotte d'Incamps B, Imhoff-Manuel RD, Zytnicki D. Early intrinsic hyperexcitability does not contribute to motoneuron degeneration in amyotrophic lateral sclerosis. Elife. 2014; 3

Li JY, Plomann M, Brundin P. Huntington's disease: a synaptopathy? Trends Mol Med. 2003; 9:414–420. [PubMed: 14557053]

Ling KK, Lin MY, Zingg B, Feng Z, Ko CP. Synaptic defects in the spinal and neuromuscular circuitry in a mouse model of spinal muscular atrophy. PLoS One. 2010; 5:e15457. [PubMed: 21085654]

Liu H, Lu J, Chen H, Du Z, Li XJ, Zhang SC. Spinal muscular atrophy patient-derived motor neurons exhibit hyperexcitability. Sci Rep. 2015; 5:12189. [PubMed: 26190808]

Lotti F, Imlach WL, Saieva L, Beck ES, Hao le T, Li DK, Jiao W, Mentis GZ, Beattie CE, McCabe BD, et al. An SMN-dependent U12 splicing event essential for motor circuit function. Cell. 2012; 151:440–454. [PubMed: 23063131]

Lu W, Bushong EA, Shih TP, Ellisman MH, Nicoll RA. The cell-autonomous role of excitatory synaptic transmission in the regulation of neuronal structure and function. Neuron. 2013; 78:433–439. [PubMed: 23664612]

Makhortova NR, Hayhurst M, Cerqueira A, Sinor-Anderson AD, Zhao WN, Heiser PW, Arvanites AC, Davidow LS, Waldon ZO, Steen JA, et al. A screen for regulators of survival of motor neuron protein levels. Nat Chem Biol. 2011; 7:544–552. [PubMed: 21685895]

Marcello E, Epis R, Saraceno C, Di Luca M. Synaptic dysfunction in Alzheimer's disease. Adv Exp Med Biol. 2012; 970:573–601. [PubMed: 22351073]

Martinez TL, Kong L, Wang X, Osborne MA, Crowder ME, Van Meerbeke JP, Xu X, Davis C, Wooley J, Goldhamer DJ, et al. Survival motor neuron protein in motor neurons determines synaptic integrity in spinal muscular atrophy. J Neurosci. 2012; 32:8703–8715. [PubMed: 22723710]

Mazarakis NK, Cybulska-Klosowicz A, Grote H, Pang T, Van Dellen A, Kossut M, Blakemore C, Hannan AJ. Deficits in experience-dependent cortical plasticity and sensory-discrimination learning in presymptomatic Huntington's disease mice. J Neurosci. 2005; 25:3059–3066. [PubMed: 15788762]

McGovern VL, Iyer CC, Arnold WD, Gombash SE, Zaworski PG, Blatnik AJ 3rd, Foust KD, Burghes AH. SMN expression is required in motor neurons to rescue electrophysiological deficits in the SMNDelta7 mouse model of SMA. Hum Mol Genet. 2015; 24:5524–5541. [PubMed: 26206889]

Mentis GZ, Blivis D, Liu W, Drobac E, Crowder ME, Kong L, Alvarez FJ, Sumner CJ, O'Donovan MJ. Early functional impairment of sensory-motor connectivity in a mouse model of spinal muscular atrophy. Neuron. 2011; 69:453–467. [PubMed: 21315257]

Mentis GZ, Diaz E, Moran LB, Navarrete R. Early alterations in the electrophysiological properties of rat spinal motoneurones following neonatal axotomy. J Physiol. 2007; 582:1141–1161. [PubMed: 17510183]

Meredith GE, Kang UJ. Behavioral models of Parkinson's disease in rodents: a new look at an old problem. Mov Disord. 2006; 21:1595–1606. [PubMed: 16830310]

Milnerwood AJ, Raymond LA. Corticostriatal synaptic function in mouse models of Huntington's disease: early effects of huntingtin repeat length and protein load. J Physiol. 2007; 585:817–831. [PubMed: 17947312]

Muller ML, Albin RL, Kotagal V, Koeppe RA, Scott PJ, Frey KA, Bohnen NI. Thalamic cholinergic innervation and postural sensory integration function in Parkinson's disease. Brain. 2013; 136:3282–3289. [PubMed: 24056537]

Ng SY, Soh BS, Rodriguez-Muela N, Hendrickson DG, Price F, Rinn JL, Rubin LL. Genome-wide RNA-Seq of Human Motor Neurons Implicates Selective ER Stress Activation in Spinal Muscular Atrophy. Cell Stem Cell. 2015; 17:569–584. [PubMed: 26321202]

O'Donnell P. Cortical interneurons, immune factors and oxidative stress as early targets for schizophrenia. Eur J Neurosci. 2012; 35:1866–1870. [PubMed: 22708597]

Osborne M, Gomez D, Feng Z, McEwen C, Beltran J, Cirillo K, El-Khodor B, Lin MY, Li Y, Knowlton WM, McKemy DD, Bogdanik L, Butts-Dehm K, Martens K, Davis C, Doty R, Wardwell K, Ghavami A, Kobayashi D, Ko CP, Ramboz S, Lutz C. Characterization of behavioral and neuromuscular junction phenotypes in a novel allelic series of SMA mouse models. Hum Mol Genet. 2012; 21:4431–4447. [PubMed: 22802075]

Palop JJ, Chin J, Mucke L. A network dysfunction perspective on neurodegenerative diseases. Nature. 2006; 443:768–773. [PubMed: 17051202]

Palop JJ, Chin J, Roberson ED, Wang J, Thwin MT, Bien-Ly N, Yoo J, Ho KO, Yu GQ, Kreitzer A, et al. Aberrant excitatory neuronal activity and compensatory remodeling of inhibitory hippocampal circuits in mouse models of Alzheimer's disease. Neuron. 2007; 55:697–711. [PubMed: 17785178]

Palop JJ, Mucke L. Amyloid-beta-induced neuronal dysfunction in Alzheimer's disease: from synapses toward neural networks. Nat Neurosci. 2010; 13:812–818. [PubMed: 20581818]

Park GH, Maeno-Hikichi Y, Awano T, Landmesser LT, Monani UR. Reduced survival of motor neuron (SMN) protein in motor neuronal progenitors functions cell autonomously to cause spinal muscular atrophy in model mice expressing the human centromeric (SMN2) gene. J Neurosci. 2010; 30:12005–12019. [PubMed: 20826664]

Port RG, Gandal MJ, Roberts TP, Siegel SJ, Carlson GC. Convergence of circuit dysfunction in ASD: a common bridge between diverse genetic and environmental risk factors and common clinical electrophysiology. Front Cell Neurosci. 2014; 8:414. [PubMed: 25538564]

Powers RK, Binder MD. Input-output functions of mammalian motoneurons. Rev Physiol Biochem Pharmacol. 2001; 143:137–263. [PubMed: 11428264]

Quinlan KA, Schuster JE, Fu R, Siddique T, Heckman CJ. Altered postnatal maturation of electrical properties in spinal motoneurons in a mouse model of amyotrophic lateral sclerosis. J Physiol. 2011; 589:2245–2260. [PubMed: 21486770]

Roselli F, Caroni P. A circuit mechanism for neurodegeneration. Cell. 2012; 151:250–252. [PubMed: 23063119]

Sareen D, Ebert AD, Heins BM, McGivern JV, Ornelas L, Svendsen CN. Inhibition of apoptosis blocks human motor neuron cell death in a stem cell model of spinal muscular atrophy. PLoS One. 2012; 7:e39113. [PubMed: 22723941]

Saxena S, Caroni P. Selective neuronal vulnerability in neurodegenerative diseases: from stressor thresholds to degeneration. Neuron. 2011; 71:35–48. [PubMed: 21745636]

Sigurdsson T. Neural circuit dysfunction in schizophrenia: Insights from animal models. Neuroscience. 2015

Tisdale S, Pellizzoni L. Disease Mechanisms and Therapeutic Approaches in Spinal Muscular Atrophy. J Neurosci. 2015; 35:8691–8700. [PubMed: 26063904]

Uhlhaas PJ, Singer W. Neuronal dynamics and neuropsychiatric disorders: toward a translational paradigm for dysfunctional large-scale networks. Neuron. 2012; 75:963–980. [PubMed: 22998866]

Umemiya M, Araki I, Kuno M. Electrophysiological properties of axotomized facial motoneurones that are destined to die in neonatal rats. J Physiol. 1993; 462:661–678. [PubMed: 8392577]

Usdin MT, Shelbourne PF, Myers RM, Madison DV. Impaired synaptic plasticity in mice carrying the Huntington's disease mutation. Hum Mol Genet. 1999; 8:839–846. [PubMed: 10196373]

Vucic S, Nicholson GA, Kiernan MC. Cortical hyperexcitability may precede the onset of familial amyotrophic lateral sclerosis. Brain. 2008; 131:1540–1550. [PubMed: 18469020]

Wainger BJ, Kiskinis E, Mellin C, Wiskow O, Han SS, Sandoe J, Perez NP, Williams LA, Lee S, Boulting G, et al. Intrinsic membrane hyperexcitability of amyotrophic lateral sclerosis patient-derived motor neurons. Cell Rep. 2014; 7:1–11. [PubMed: 24703839]

Wichterle H, Lieberam I, Porter JA, Jessell TM. Directed differentiation of embryonic stem cells into motor neurons. Cell. 2002; 110:385–397. [PubMed: 12176325]

Yasuda T, Nakata Y, Choong CJ, Mochizuki H. Neurodegenerative changes initiated by presynaptic dysfunction. Transl Neurodegener. 2013; 2:16. [PubMed: 23919415]

Yin J, Yuan Q. Structural homeostasis in the nervous system: a balancing act for wiring plasticity and stability. Front Cell Neurosci. 2014; 8:439. [PubMed: 25653587]

Zeron MM, Hansson O, Chen N, Wellington CL, Leavitt BR, Brundin P, Hayden MR, Raymond LA. Increased sensitivity to N-methyl-D-aspartate receptor-mediated excitotoxicity in a mouse model of Huntington's disease. Neuron. 2002; 33:849–860. [PubMed: 11906693]

Zoghbi HY, Bear MF. Synaptic dysfunction in neurodevelopmental disorders associated with autism and intellectual disabilities. Cold Spring Harb Perspect Biol. 2012; 4

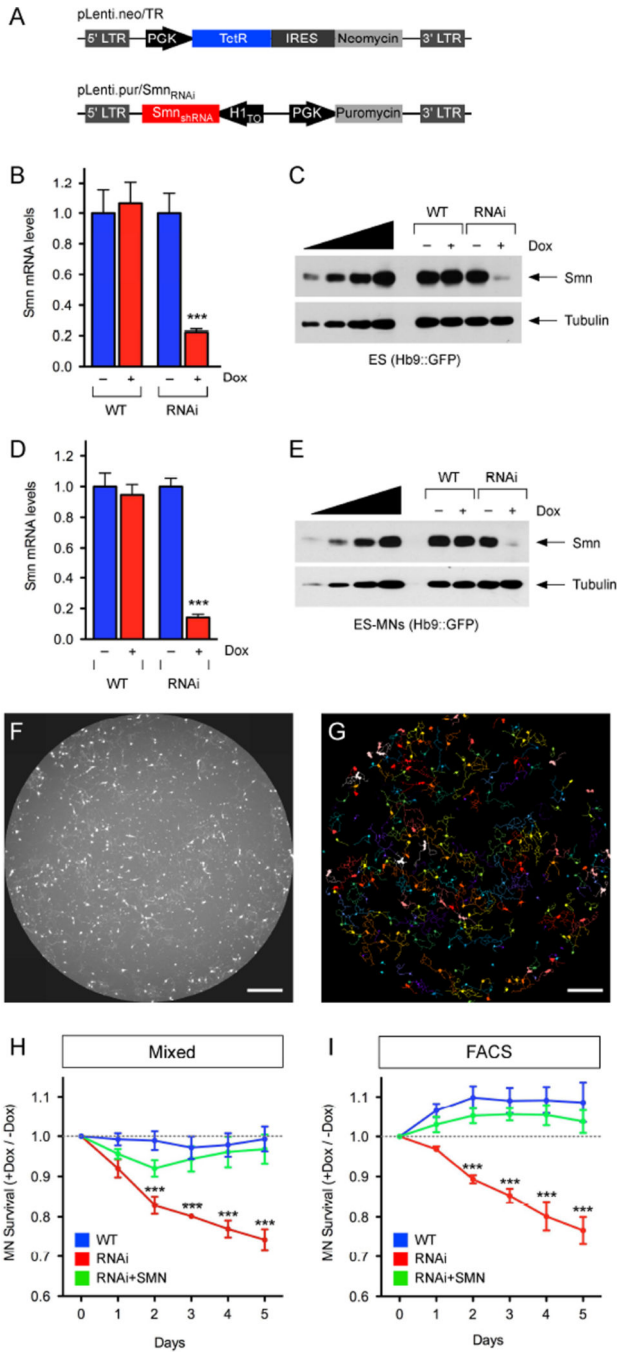

Figure 1. Smn deficiency induces MN death through cell autonomous mechanisms

(A) Schematic representation of the lentiviral vectors used to generate the ES(Hb9:GFP)-Smn_{RNAi} cell line. (B) RT-qPCR analysis of Smn mRNA levels in WT and RNAi ES cells cultured with and without Dox for 4 days. RNA levels in Dox-treated cells are expressed relative to those in untreated cells. Data are represented as mean and SEM from independent experiments (n=3). (C) Western blot analysis of Smn protein levels in WT and RNAi ES cells cultured with and without Dox for 4 days. A two-fold serial dilution of WT ES cell extract is analyzed on the left. (D) RT-qPCR analysis of Smn mRNA levels in FACS-purified

MNs differentiated from WT and RNAi ES cells cultured with and without Dox for 5 days. RNA levels in Dox-treated cells are expressed relative to those in untreated cells. Data are represented as mean and SEM from independent experiments (n=3). (E) Western blot analysis of Smn protein levels in mixed cultures of ES-MNs cultured with and without Dox for 5 days after differentiation from WT and RNAi ES cells. A two-fold serial dilution of the extract from WT ES-MNs is analyzed on the left. (F) Representative 96-well image of GFP+ MNs differentiated from WT ES cells at 5DIV. Scale bar=800μm. (G) MetaMorph software analysis of GFP+ MNs from the image in F. Scale bar=800μm. (H) Survival analysis of GFP + MNs in mixed cultures following differentiation from WT, RNAi and RNAi+SMN ES cells cultured with and without Dox. Normalized data of Dox-treated relative to untreated cells are shown as mean and SEM from independent experiments (n≥6). (I) Survival analysis of FACS purified GFP+ MNs following differentiation from WT, RNAi and RNAi+SMN ES cells cultured with and without Dox. Normalized data of Dox-treated relative to untreated cells are shown as mean and SEM from independent experiments (n=3). See also Figure S1.

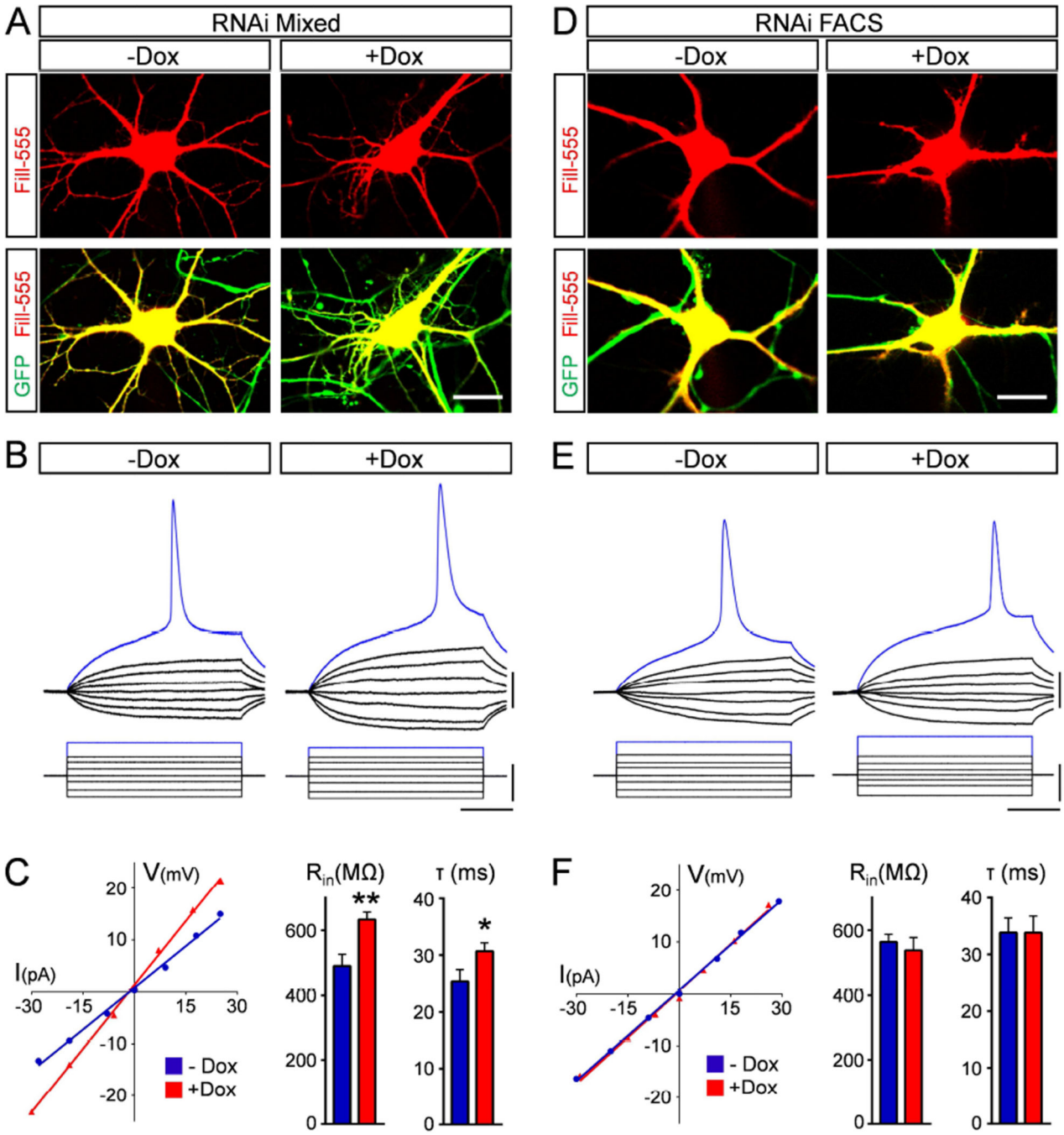

Figure 2. Smn deficiency induces MN hyperexcitability non-cell autonomously

(A) Representative images of intracellularly filled control (−Dox) and Smn-deficient (+Dox) MNs differentiated from RNAi ES cells and cultured under mixed conditions for 5 days. Upper panel: Alexa-555 fill in red; lower panel: merged with GFP in green. Scale bar=20μm. (B) Superimposed membrane responses (upper traces) following current injection (lower traces) in control and Smn-deficient MNs as in A. Scale bars=20mV, 40pA, 40ms. (C) Current/voltage relationships for the MNs shown in B (Input resistance: −Dox= 534MΩ, +Dox= 782MΩ) and averages for input resistance (R_{in}) and time constant (τ) of

control (n=15) and Smn-deficient (n=14) MNs at 5DIV. (D) Representative images of intracellularly filled control (−Dox) and Smn-deficient (+Dox) MNs differentiated from RNAi ES cells and cultured for 5 days after FACS purification. Upper panel: Alexa-555 fill in red; lower panel: merged with GFP in green. Scale bar= 20μm. (E) Superimposed membrane responses (upper traces) following current injection (lower traces) of control and Smn-deficient FACS purified MNs as in D. Scale bars= 20mV, 40pA, 40ms. (F) Current/voltage relationships for the two FACS purified MNs shown in E (Input resistance: −Dox=582MΩ, +Dox=598MΩ) and average input resistance and time constant of FACS purified control (n=15) and Smn-deficient (n=15) MNs at 5DIV. See also Figure S2.

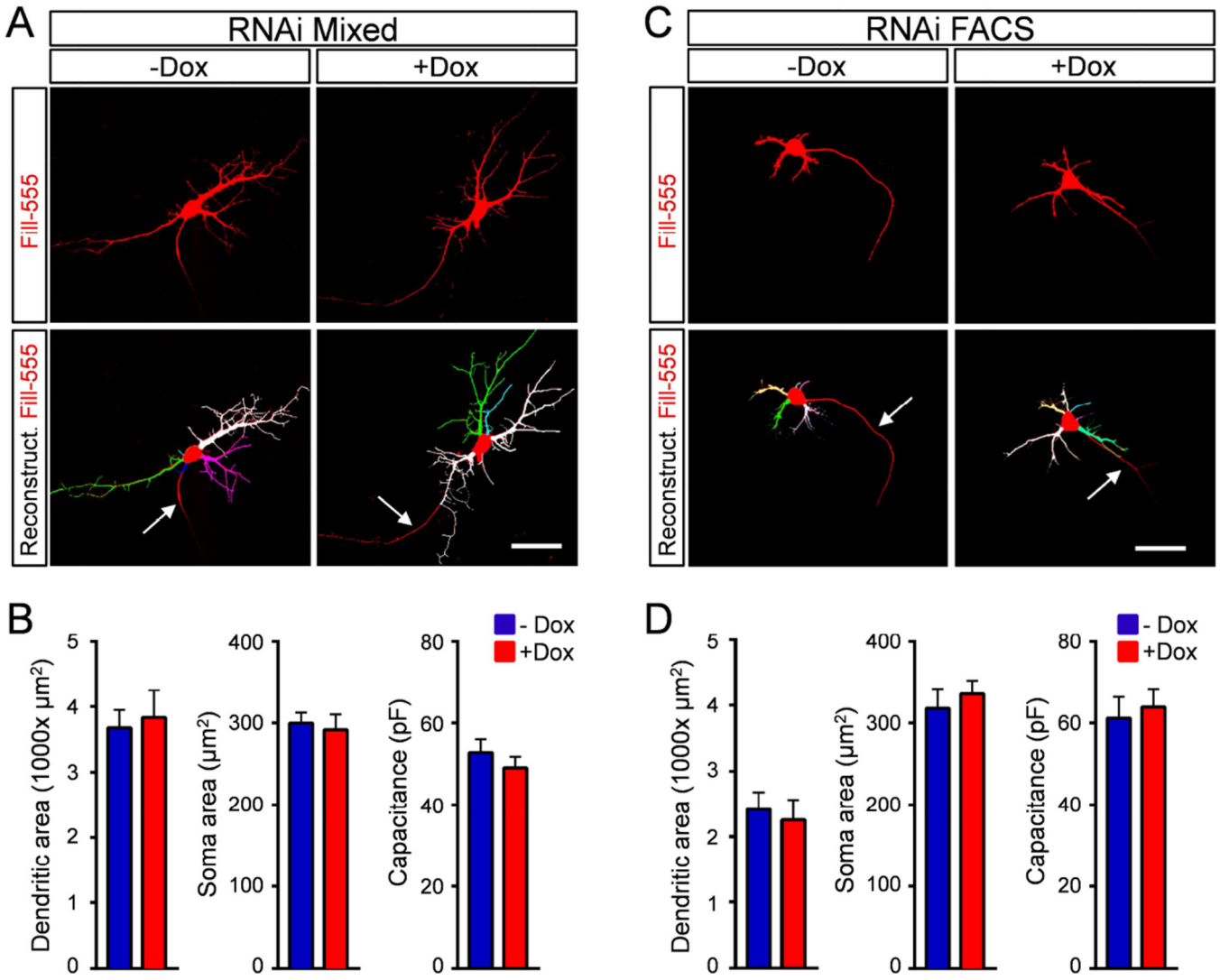

Figure 3. Smn deficiency does not alter the somato-dendritic area of MNs

(A) Single-plane confocal images of Alexa-555 intracellularly-filled control (−Dox) and Smn-deficient (+Dox) MNs differentiated from RNAi ES cells in mixed cultures at 5DIV (upper panels) and Neurolucida reconstructions of their dendritic trees (bottom panels). (B) Quantification of dendritic tree, soma area and capacitance of control (n=13) and Smn-deficient (n=12) MNs in mixed cultures at 5DIV. (C) Single-plane confocal images of Alexa-555 intracellularly-filled control (−Dox) and Smn-deficient (+Dox) FACS purified MNs differentiated from RNAi ES cells at 5DIV (upper panels) and Neurolucida reconstruction of their dendritic trees (bottom panels). (D) Quantification of dendritic tree, soma area and capacitance of control (n=9) and Smn-deficient (n=7) MNs in FACS purified cultures at 5DIV. Arrows indicate putative axons. Scale bars=40µm. See also Figure S3.

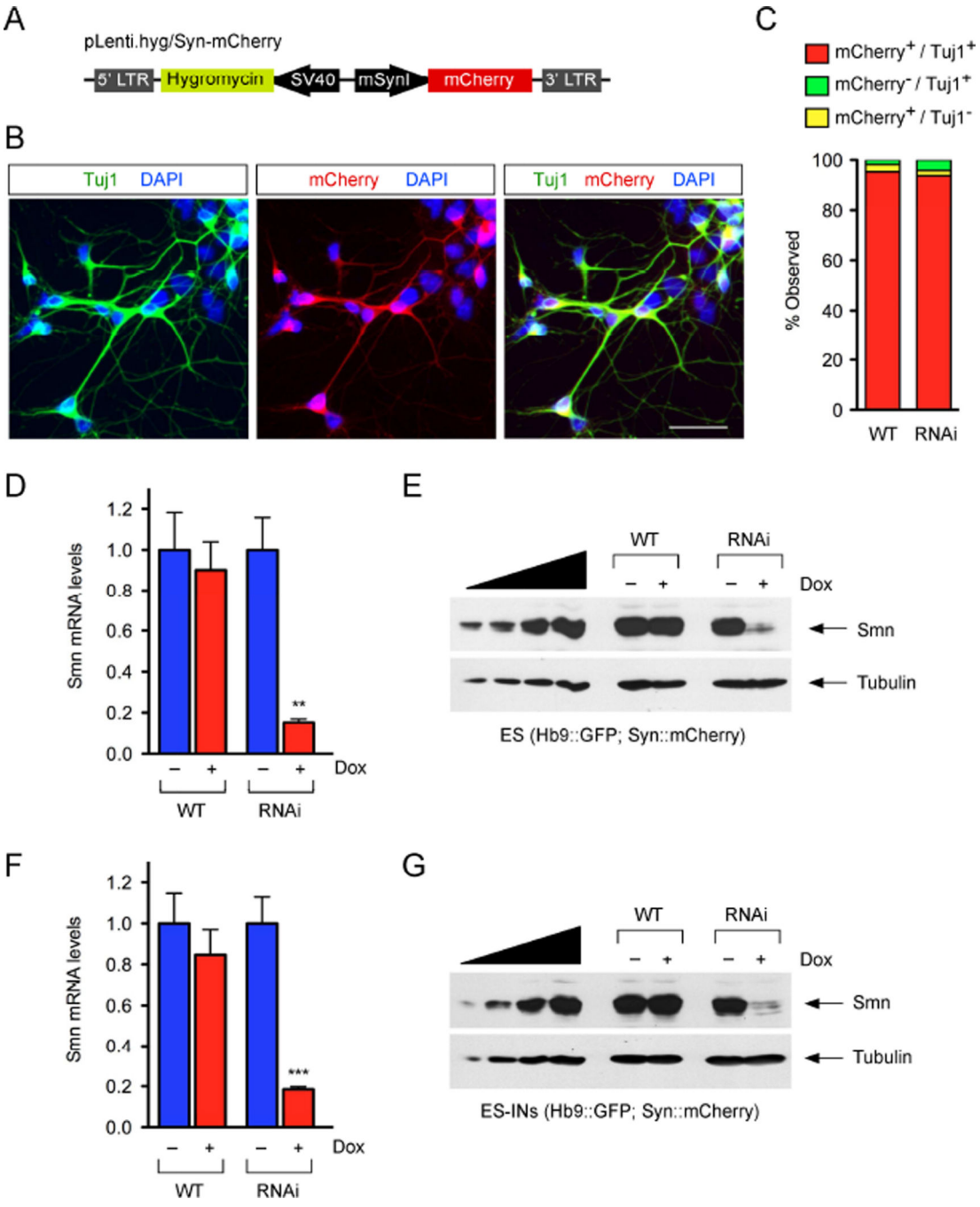

Figure 4. Development of ES cell lines for the purification of INs with inducible Smn knockdown

(A) Schematic representation of the lentiviral vector used to generate WT and RNAi ES(Hb9::GFP;Syn::mCherry) cell lines. (B) Representative images of ES(Hb9::GFP;Syn::mCherry)-derived neuronal cultures expressing mCherry (red) and stained with Tuj1 (green) and DAPI (blue) at 5DIV. (C) Quantification of mCherry+/Tuj1+ INs in neuronal cultures differentiated from WT and RNAi ES(Hb9::GFP;Syn::mCherry) cells as in B (n≥3). Scale bar=100μm. (D) RT-qPCR analysis of Smn mRNA levels in WT and RNAi ES(Hb9::GFP;Syn::mCherry) cells cultured with and without Dox for 4 days.

RNA levels in Dox-treated cells are expressed relative to those in untreated cells. Data are represented as mean and SEM from independent experiments (n=3). (E) Western blot analysis of Smn protein levels in WT and RNAi ES cells cultured as in D. A two-fold serial dilution of WT ES cell extract is analyzed on the left. (F) RT-qPCR analysis of Smn mRNA levels in FACS-purified INs differentiated from WT and RNAi ES cells cultured with and without Dox for 5 days. RNA levels in Dox-treated cells are expressed relative to those in untreated cells. Data are represented as mean and SEM from independent experiments (n=3). (G) Western blot analysis of Smn protein levels in mixed cultures of ES-INs cultured with and without Dox for 5 days after differentiation from WT and RNAi ES cells. A two-fold serial dilution of the extract from WT ES-INs is analyzed on the left. See also Figure S4.

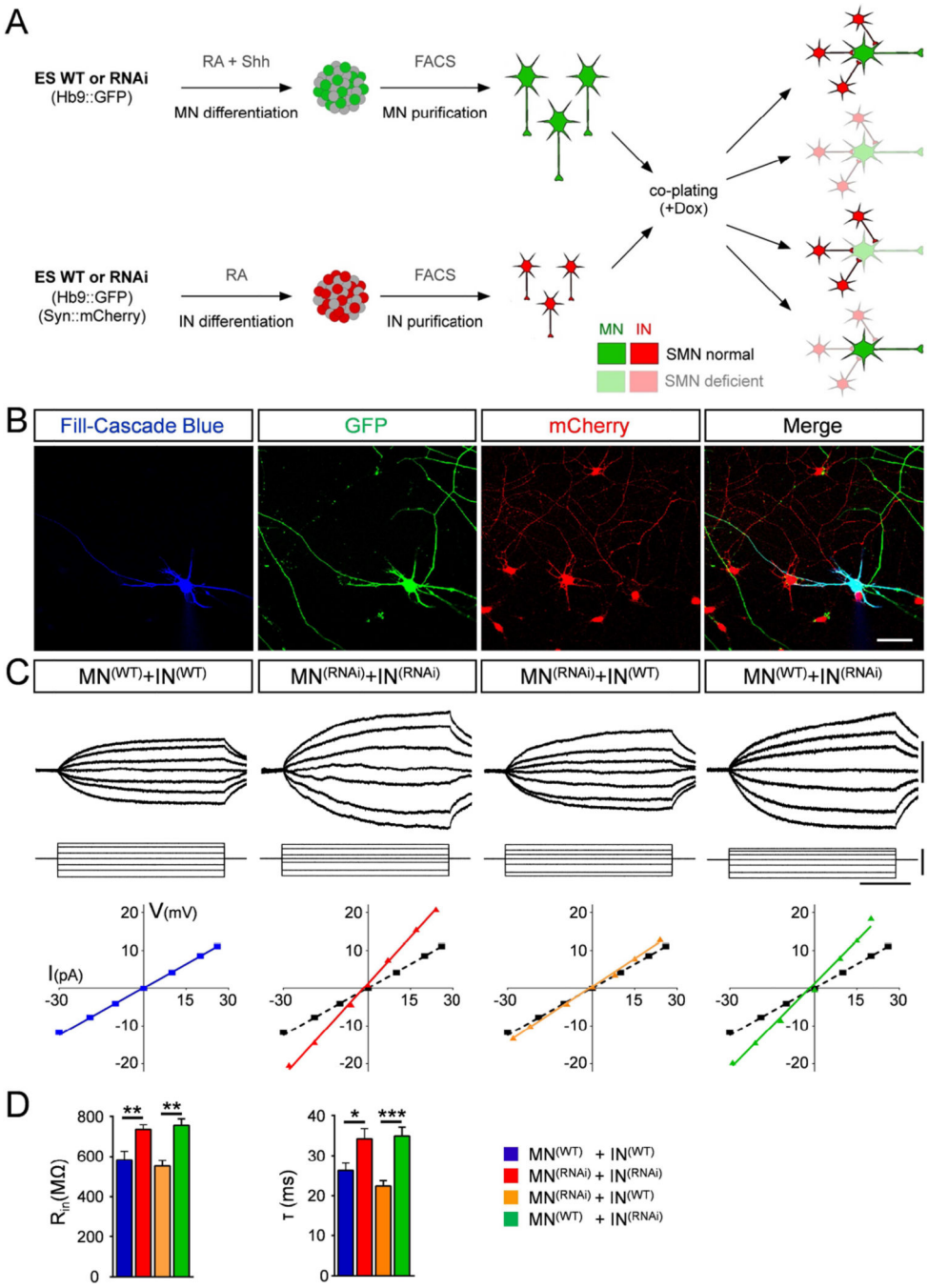

Figure 5. Smn deficiency in pre-motor INs induces MN hyperexcitability

(A) Schematic representation of the design for co-culture experiments with FACS purified MNs and INs. (B) Representative confocal images of an intracellularly filled (blue), GFP^+ (green) MN co-cultured with $mCherry^+$ (red) INs. Scale bar=50μm. (C) Superimposed membrane responses (upper traces) following current injection (lower traces) and current/voltage relationships for MNs recorded in all four combinations. Scale bars=20mV, 40pA, 40ms. For ease of comparison, in each graph the black dotted line represents the current/voltage relationship under wild-type conditions. (D) Mean input resistance (R_{in}) and time

constant (τ) of MNs recorded in the four different combinations. MN(WT)+IN(WT), n=12; MN(RNAi)+IN(RNAi), n=13; MN(RNAi)+IN(WT), n=18; MN(WT)+IN(RNAi), n=17. See also Figure S5.

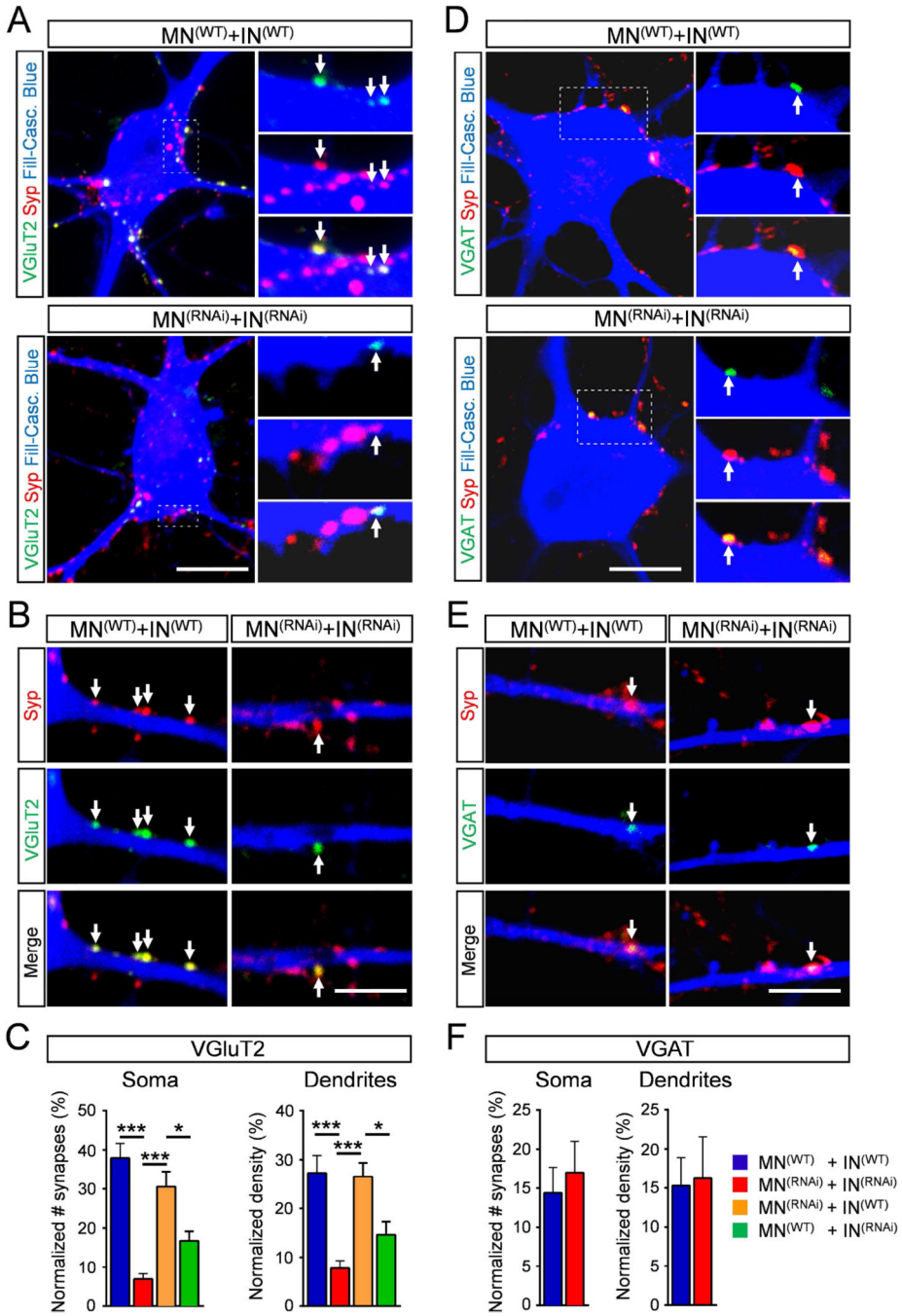

Figure 6. Smn deficiency in INs leads to loss of excitatory synapses onto MNs

(A–B) Superimposed images of VGluT2 (green) and Syp (red) immunoreactivity on the soma and the dendrites of a Cascade blue intracellularly-filled MN (blue) in co-cultures of MNs and INs differentiated from either WT or RNAi ES cells as indicated. Arrows indicate VGluT2 synapses. (C) Number of VGluT2 synapses relative to all Syp^{+} synapses onto the soma and dendrites of MNs from all four co-culture combinations. MN(WT)+IN(WT), n=11; MN(RNAi)+IN(RNAi), n=12; MN(RNAi)+IN(WT), n=10; MN(WT)+IN(RNAi, n=10. (D–E) Superimposed images of VGAT (green) and Syp (red) immunoreactivity on the

soma and the dendrites of MNs as in A. Arrows indicate VGAT synapses. (F) Number of VGAT synapses relative to all Syp^+ synapses onto the soma and dendrites of MNs from two co-culture combinations. MN(WT)+IN(WT), n=8; MN(RNAi)+IN(RNAi), n=7. Scale bar=10μm (soma) and 5μm (dendrites). See also Figure S6.

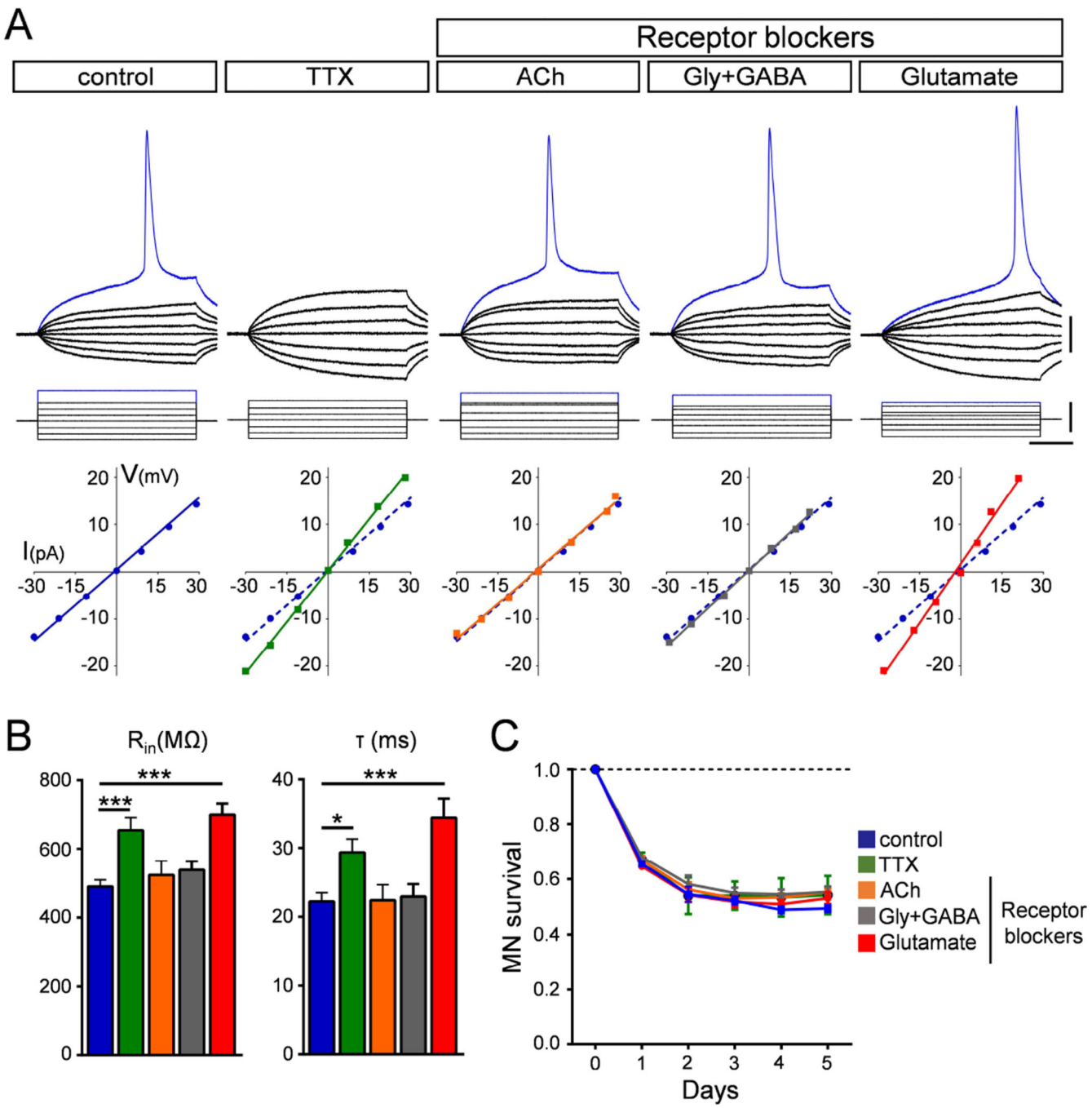

Figure 7. Block of excitatory neurotransmission induces hyperexcitability but not death of MNs

(A) Superimposed membrane responses (upper traces) following current injection (lower traces) of WT MNs in mixed cultures under different pharmacological conditions. Graphs show current/voltage relationships for the corresponding MNs in each treatment group. The current/voltage relationship of the control MN (blue dotted line) is included in each graph for ease of comparison. Scale bars=20mV, 40pA, 40ms. (B) Mean input resistance (R_{in}) and time constant (τ) for all experimental groups. Number of recorded MNs: control, n=24; TTX, n=15; Ach blockers, n=12, Gly+GABA blockers, n=13, Glu blockers, n=11. (C)

Survival curves of MNs for all experimental groups normalized to day 0. Data represent mean and SEM from independent experiments (n=3). See also Figure S7.